The New Chapter of Transonic Compressor Cascade Design at the DLR

Edwin J. Munoz Lopez[1]
Institute of Propulsion Technology,
German Aerospace Center (DLR),
Linder Höhe, Cologne 51147, Germany
e-mail: edwin.munozlopez@dlr.de

Alexander Hergt
Institute of Propulsion Technology,
German Aerospace Center (DLR),
Linder Höhe, Cologne 51147, Germany
e-mail: alexander.hergt@dlr.de

Sebastian Grund
Institute of Propulsion Technology,
German Aerospace Center (DLR),
Linder Höhe, Cologne 51147, Germany
e-mail: sebastian.grund@dlr.de

Volker Gümmer
Chair of Turbomachinery and Flight Propulsion,
Department of Aerospace and Geodesy,
Technical University of Munich,
Boltzmann Street. 15,
Garching 85748, Germany
e-mail: volker.guemmer@tum.de

The design of compressor blades has been transformed by the advent of optimization algorithms, allowing designers to focus on finding the best optimization strategy for a desired application. However, transonic flow conditions on compressor blades still present considerable modeling challenges, even for a 2D blade section. This paper then focuses on the design of a new state-of-the-art compressor cascade for future test campaigns at the DLR's Transonic Cascade Wind Tunnel (TGK). For this purpose, a review of the cascades previously tested at the TGK was performed to select a main reference with good efficiency at high loading. The data gathered also informed the optimization strategy applied with the DLR's optimizer, AutoOpti. The process chain was evaluated with Reynolds Averaged Navier–Stokes CFD simulations using the DLR's solver, TRACE. The optimization was set to minimize two objective functions: the first one focused on the efficiency at the design point, and the second one focused on the efficiency over the working range. The result is a Pareto front of cascades with a wide variety of design features with an efficiency improvement over the working range of about 24%. This improvement was achieved with a comparable aerodynamic loading. Further analyses were performed to select the "best" cascade for future test campaigns. The significant improvement obtained with respect to the reference and the wide variety of designs observed demonstrates that there is still much to be learned about blade design through optimization; even for 2D cascades and specially in transonic flow. [DOI: 10.1115/1.4056982]

Keywords: computational fluid dynamics (CFD), fan, compressor, and turbine aerodynamic design, turbomachinery blading design

1 Introduction

Airfoil design methodologies have evolved drastically over the last decades. Initially, the design task would involve a methodical exploration of a family of airfoil shapes. This process would be supported by the gathering of empirical knowledge, correlations, and professional experience in airfoil design and performance. Over time, the design process was improved with the introduction of viscous–inviscid interaction algorithms and inverse design tools that allowed the design of so-called controlled diffusion airfoils. Today, the advent of advanced numerical optimization techniques and increased computing power has shifted the focus of designers toward the exploration of parametrization and optimization strategies for different design requirements. For compressor cascades, these requirements are generally driven by the continuous search for improvements on the efficiency and pressure ratio at the Design Point (DP) and over the Working Range (WR) within a given set of operating conditions.

Nowadays, a considerable amount of literature can be found regarding the optimization of compressor blades, with different approaches and results. A test case frequently observed in the literature on this topic is the optimization of NASA's Rotor 37, as summarized in Ref. [1]. In this study, the optimization design system by Rolls-Royce plc, *SOPHY* [2], is applied with a free-form deformation technique, considerably improving the rotor's efficiency. Further improvement was obtained in Ref. [3] using Cenaero's optimizer, *MINEMA* [4], with a similar parametrization approach and additional degrees-of-freedom. However, this approach considerably affected the choking behavior of the rotor, especially at off-design conditions. On the other hand, more conventional parametrization approaches with single and multi-objective algorithms have also achieved notable improvements in efficiency, while maintaining the rotor's operation much closer to the original design, as shown in Refs. [5,6]. This exemplifies some of the typical trade-offs between the optimization approach and the priorities of the design effort.

The German Aerospace Center's (DLR) Institute of Propulsion Technology also counts on an in-house optimization suite named *AutoOpti*. This multi- objective optimizer is based on evolutionary algorithms supported by surrogate models to accelerate the convergence of the optimization. It was first introduced in Ref. [7] to improve the performance of a highly-loaded low-pressure compressor blade. Since then, it has been further developed and applied in numerous studies related to the design of compressor machines, such as in Refs. [8–10]. In many of these publications, an existing design is again used as a starting point with the objective of improving the efficiency of the rotor, while maintaining its performance and operational features. More generally, AutoOpti was utilized in Ref. [11] to produce a database of airfoils optimized for different applications within a compressor machine. The optimization approach is then adjusted by defining the design space for the corresponding requirement space, once again showing how different design goals may benefit from different optimization approaches.

However, a key common feature of the aforementioned investigations is the trade-off between the parametrization approach and the fidelity of the flow solver employed. The extensive amount of parameters required to define a 2D compressor blade section, let alone the entire blade itself, results in an exponential increase of the computational resources required to run the optimization. The result is that many studies either employ RANS CFD simulations with a simplified 2D parametrization of the blade sections or resort to modern viscous–inviscid interaction flow solvers of lower fidelity such as *MISES* [12]. Even though the latter algorithms have been shown to provide quick and reliable results for subsonic

[1]Corresponding author.

Contributed by the International Gas Turbine Institute (IGTI) of ASME for publication in the Journal of Turbomachinery. Manuscript received July 26, 2022; final manuscript received January 19, 2023; published online April 3, 2023. Assoc. Editor: David G. Bogard.

cascades, transonic operating conditions still present considerable modeling challenges. These include solver stability, as discussed in Ref. [11], and also difficulties in fully capturing the effects of Shock-Boundary Layer Interaction (SBLI) and sidewall contraction that drastically influence the properties of the flow around the 2D cascade. Another phenomenon of high interest and complexity is the inherent unsteadiness of the SBLI in terms of amplitude and frequency of shock oscillation. Unfortunately, properly capturing these features has been shown to require even higher fidelity CFD methods. This is still outside the scope of an optimization effort and to this day forces designers to trade performance for overly conservative design margins, as established in Ref. [13].

In order to address these challenges, the DLR has joined the EU-funded consortium, *Towards Effective Flow Control and Mitigation of Shock Effects in Aeronautical Applications (TEAMAero)*. The DLR's objective within the consortium consists of designing a new state-of-the-art 2D transonic compressor cascade on which to investigate, through numerical and experimental means, the origin and mitigation of said unsteady SBLI phenomenon. This publication is then dedicated to the design of the new cascade through the use of advanced optimization software, an integrated RANS CFD solver, and a set of 21 design parameters dedicated to fully describe the cascade's geometrical properties. This paper then begins by discussing the progression of transonic compressor cascade designs as observed over five decades of wind tunnel testing at the DLR. Subsequently, the numerical tools and design methods employed to achieve the design goal are presented. Afterward, the design point and design space defined for the optimization are discussed. This is followed by a detailed description of the airfoil design strategy and the optimization process chain. Finally, the results of the optimization are presented, including an analysis of the cascade candidates available, and complementary analyses performed to determine the "best" design for the new cascade.

2 Five Decades of Transonic Compressor Cascade Testing at the DLR

The DLR's Transonic Cascade Wind Tunnel (TGK) in Cologne has a vast history as one of the leading institutions in Europe for linear cascade testing [14]. Over the years, an extensive catalog of subsonic and transonic compressor cascades has been tested at this facility with top-of-the-line measurement techniques. For this reason, the first step before attempting to design a new state-of-the-art transonic compressor cascade was to perform a thorough review of similar cascades tested at the TGK from the 1970s. Within this timeframe, over 20 different cascades were tested in transonic flow conditions. This cascade catalog includes in-house DLR designs created for research investigations, but also many designs provided by industrial partners, including Rolls- Royce, MTU Aero Engines, and others. Therefore, the progression of compressor cascade design methodologies over the years can be clearly observed through this catalog.

From as early as the 1970s and most of the 1980s, compressor airfoils for high Mach number applications were based on circular arc design methodologies. For these airfoils, the suction and pressure surfaces were defined by either two circular arcs of different radii for Double Circular Arc (DCA) airfoils or multiple arcs for Multiple Circular Arc (MCA) airfoils. Accordingly, in 1976, the DLR systematically investigated two such types of cascades obtained from different sections of a transonic rotor to pioneer a new understanding of the effect of Axial Velocity Density Ratio (AVDR) on transonic cascade performance [15]. This study was complemented by multiple investigations of the L030 rotor designed with DCA and MCA airfoils at the DLR with the methodologies available at the time [16–19]. These methodologies would be considered conservative today, as they were based on correlations and empirical data from the study of different series of comparable airfoils. However, these cascades still provide a good reference for the current study.

From the late 1980s, design methodologies evolved with the introduction of efficient and relatively reliable viscous–inviscid interaction algorithms. The introduction of these algorithms allowed designers to manually optimize the shape of the cascades. Inverse design methodologies were also now available to help designers achieve a prescribed velocity distribution around the airfoil, also referred to as controlled diffusion airfoils, as explained in Ref. [20]. The DLR once again was at the forefront of these developments, as the new techniques were applied in Ref. [21] to successfully improve the design of the L030 rotor sections from previous studies with the TSG89-5 cascade. Similar methods were also applied successfully to achieve the design goals of a propfan cascade, as presented in Ref. [22]. However, another effort at the DLR aimed at increasing the aerodynamic loading as much as possible for the design of the TSG91-8k cascade in Ref. [23] yielded mixed results. In this study, the cascade failed to deliver the performance expected from the numerical simulations in the experiments due to the unexpected separation of the boundary layer near the trailing edge. Nevertheless, these designs and their variations helped the DLR advance the knowledge of linear cascade testing in transonic conditions in Refs. [21,24–26].

Since the 2000s, developments in measurement techniques have allowed the DLR to study in detail the flow around the transonic compressor cascades provided by industrial partners. These studies were for instance focused on the effect of leading-edge degradation in Ref. [27] or on the study of SBLI behavior in Refs. [13,28]. Over the course of this time, a new wave of efficient CFD flow solvers and automated optimization algorithms have been introduced that allow the efficient exploration of more designs than ever before. Thanks to the aforementioned AutoOpti software suite, the DLR has also been involved in advancing the knowledge of these methodologies. However, this study aims to fill the current gap at the institute, by utilizing these new design tools to define a new transonic compressor cascade comparable to the state-of-the-art currently available in the industry. This cascade is intended to serve as a canvas for the future study of flow control methods of unsteady SBLI phenomena at the TGK. Therefore, this design is not meant to be applied to a specific compressor machine, but instead to help the research community advance the fundamental understanding of the phenomena that hold back the performance of the compressor blade designs available today. A compilation of the cascades discussed in this section in terms of Flow Turning (FT) versus inlet Mach number can be observed in Fig. 1.

3 Design Methods

For this optimization, a three-step process chain was set up in order to generate the airfoil, mesh the cascade, and perform CFD simulations and post-process the results of interest. The results of

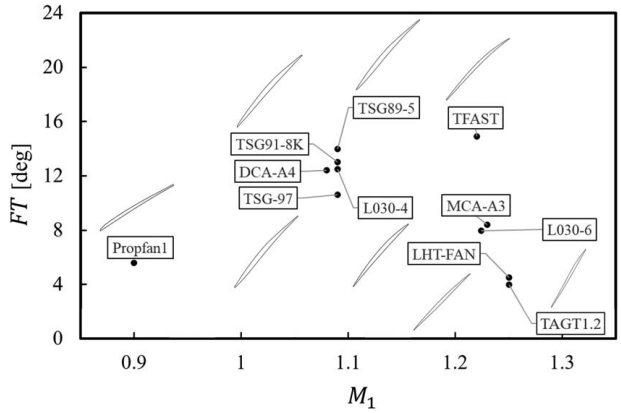

Fig. 1 Transonic cascades tested at the TGK

the process chain were then routed to the optimizer, which also served as the interface during the whole process. For each step, different numerical methods available in-house at the DLR were employed. In this section, these methods are presented and described in detail.

3.1 BladeGen: Airfoil Geometry Parametrization. The parametrization of the cascade is done through the software, *BladeGen*, first introduced in Ref. [7]. The suction and pressure surfaces are built with cubic B-Splines defined with five Control Points (CP) each for this study. The Leading Edge (LE) and Trailing Edge (TE) set the first and last CP on each surface and are defined themselves by a radius (r), an elliptical parameter (AB), and their angles with respect to the unstaggered horizontal axis (β). The LE has an additional parameter to define an amount of asymmetry. On the suction surface, the second and second last CPs are defined based on the angle difference ($\Delta\beta$) with respect to the LE and TE angles, respectively, and the unstaggered horizontal coordinate (x). The remaining suction surface CP is defined freely by its unstaggered coordinates (x, y). The pressure side surface CPs are then defined by coordinates tangential and perpendicular to the suction side surface previously defined (m, d). This helps prevent unfeasible designs or conflicts between the CPs from both sides. Finally, the different sections are joined together, while ensuring G2 curvature continuity. Two more degrees-of-freedoms related to the cascade, the stagger angle (β_{st}) and the pitch (s), are then added before meshing. All these design parameters amount to a total of 21 degrees-of-freedom to fully define the geometry of the cascade. The entire parametrization approach described is summarized in Fig. 2 with a modified NACA 6409 airfoil.

3.2 PyMesh: Cascade Meshing. The cascade is meshed with the software, *PyMesh*, described in Ref. [29]. PyMesh is able to generate multi-block OCH grid topologies of hexahedral elements: the O block wraps around the airfoil; the C block covers a second area around the airfoil before the trailing edge; the H blocks cover the inlet, passage, and outlet zones. The software input includes the number of points, size of the elements, edge angles, and other parameters to fully define the mesh around the geometry. The input values are normalized with the chord, and some of them were linked to BladeGen parameters to ensure the mesh was always well adapted to the different airfoil geometries possible.

Another point of interest for the optimization was focused on finding a method to match the AVDR required for the cascade. This parameter defines the sidewall area contraction due to the presence of the sidewall boundary layer [30–32]. In order to numerically obtain the desired AVDR for the simulations, the wall at the "tip" of the blade is contoured over the span of the airfoil's chord to have the area contraction desired. The contoured wall is passed into PyMesh in the form of a 2D spanwise mesh, which is able to leverage it with the airfoil input to produce the final 3D mesh of the blade. The "tip" wall boundary is then defined as a slip-wall, while the "hub" of the blade as a symmetry plane. The latter then also becomes the plane at which the results of the cascade are measured.

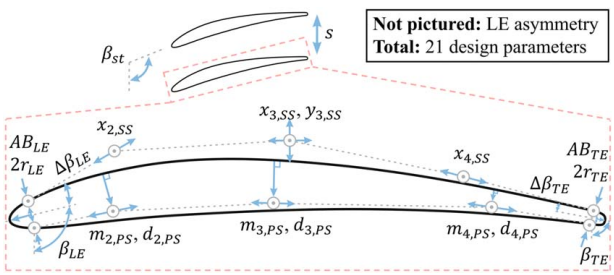

Fig. 2 BladeGen cascade parametrization

3.3 TRACE: Computational Fluid Dynamic Flow Solver. For the calculation of the flow through the cascade, the well-established in-house parallel solver for turbomachinery flows, *TRACE*, is used [33,34]. This solver has been extensively developed over the years and is currently applied by numerous industrial and academic partners. The spatial discretization is performed with a second-order Monotonic Upstream-Centered Scheme for Conservation Laws (MUSCL), applied with a modified van Albada limiter to avoid spurious oscillations due to flow discontinuities such as shocks. The inviscid fluxes at cell faces are calculated with Roe's flux differencing splitting method [35]. For the entire investigation, including the mesh convergence study and the optimization itself, TRACE's RANS solver was applied with Menter's 2003 version of the two-equation Shear Stress Transport (SST) $k-\omega$ model coupled with Menter's 2009 version of the $\gamma - Re_{\Theta}$ transition model [36,37]. This is the same setup previously applied in Ref. [13] for the investigation of a modern transonic compressor cascade. Finally, the results of the calculations were post-processed via TRACE's own *POST* software unit or by a series of python scripts as required.

3.4 AutoOpti: Numerical Optimization. The core design optimization is performed with the DLR's software suite, *AutoOpti*, first introduced in Ref. [7]. The optimizer's core strategy is based on multi-objective asynchronous evolutionary algorithms, where new members are generated based on evolutionary operators including *mutation*, *gradient*, *differential evolution*, and *expected volume gain*. Additionally, the algorithm is accelerated with a Kriging metamodel process that creates a response surface to inform the creation of new members toward a converged solution. The process chain is set up by the user, and the interface between the different steps and software is facilitated by AutoOpti. For each new member, the process chain is evaluated until the objective function values are obtained (converged member), or one of the constraints is not met (unconverged member). New converged members with good objective values are saved and are added to the population of parent members for the creation of the next candidates. This process is repeated until the optimization can be considered converged.

Some of the main features of AutoOpti relate to the management by the master process of the requested slave processes and the database of members stored. Namely, the optimization is asynchronous, meaning that the parents for new members are selected from the current database of all evaluated members and not from the previous population. This allows for optimal handling of the resources available, as the slave processes that become free are promptly assigned a new member based on the re-evaluation of the surrogate models with said database. Additionally, each member's design parameters, objective values, and other values of interest can be stored. This approach also allows users to follow the progress of the optimization, modify the parameters of the optimization if needed, and restart the optimization without any loss of information. The collection of these features ultimately allows the optimization to benefit from the user's engineering and design know-how. Further details on these features are available in Ref. [8].

4 Design Space and Mesh Convergence

For this optimization, there is a total of 21 design parameters that fully define the cascade geometry. To be able to set a reasonable design space for all these parameters, a reference database of transonic compressor cascades is then required. This pre-optimization analysis is meant to provide a basis for comparison of the new cascade in terms of performance and heuristics for the industrial applicability of the new design. In this chapter, the reference design space database is discussed, followed by a standard mesh convergence study with more details on the numerical approach, and a comparison between the CFD results obtained for one of

the reference cascades and its experimental results previously gathered in Ref. [13].

4.1 Transonic Cascade Design Space. To define the design space for the new compressor cascade, nine of the most relevant cascades available were chosen for more detailed analyses. This includes seven cascades that are shown in Fig. 1. For all these cascades, the entire set of 21 design parameters was investigated or measured when necessary. Generally, the minimum and maximum values measured were used as the parameter's limits for the optimization. However, judgment was exercised with some parameters to either increase or decrease these limits. For instance, the minimum trailing edge radius measured was 0.18% of the chord length, and the maximum was 0.61%. In this case, the minimum radius was maintained as a hard limit due to the possible manufacturing and structural problems that may arise from an even smaller radius. The maximum radius on the other hand was reduced to 0.5%, which was considered to be sufficient for the type of cascade design desired. In terms of cascade parameters, it is worth noting that the pitch design space was set between 60 mm and 70 mm, while the stagger angle was set between 134.4 deg and 140 deg.

On top of the 21 design parameters, an additional four geometrical parameters were measured to further constrain the design space. These parameters are the maximum airfoil thickness and its position along x, as well as the airfoil area and the x-coordinate of the area centroid. These parameters helped complete the heuristics of a structurally sound and feasible design. To define the limits for these constraints, a similar process was followed by using the minimum and maximum values measured from the reference airfoils as a guide, and extending or shortening that range when deemed necessary. The result was a set of four geometrical constraints for the optimization: maximum thickness between 3.2 and 5% located between 40 and 63.5%, and an airfoil area of 2.1–4.2% with the centroid located between 44.8 and 54.4%. All lengths were normalized by the chord length of the airfoil. The set of constraints on the maximum thickness is shown as an example in Fig. 3. Lastly, the airfoils were constrained to not have any local minima in their thickness distributions to avoid unfeasible designs.

4.2 Mesh Convergence Analysis. For the following analyses, the cascade labeled as *TFAST* in Fig. 1 was used. This cascade was tested at the DLR in 2015 within the framework of the European Commission's research project: Transition Location Effect on Shock Wave Boundary Layer Interaction (TFAST) [13,38]. It was then provided by Rolls-Royce Germany for the project as a representation of the state-of-the-art in the industry. Accordingly, this cascade also stands out from the references due to the high flow turning it provides at a high inlet Mach number and with a relatively low total pressure loss coefficient (ω). For these reasons, the TFAST cascade was chosen as the reference for this mesh convergence analysis, and the following comparison with experimental results.

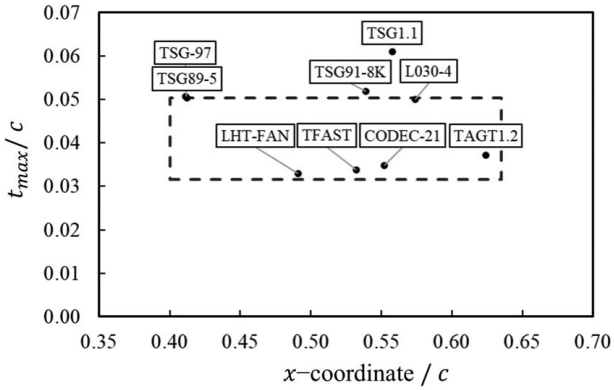

Fig. 3 Constrained design space for the maximum thickness and its position along the chord

Based on this reference, the following inputs were determined for the numerical approach based on the experimental results: at the inlet a flow angle (β_1) of 145.5 deg and an absolute total pressure (P_{01}) of 93.6 kPa; at the outlet a back pressure of 57.6 kPa; for the airfoil a chord length of 100 mm; and for the cascade an AVDR of 1.2. The chord length and AVDR inputs were also maintained for the rest of the optimization given that these are typical values of interest for transonic cascade experiments, normally leading to Reynolds numbers around 10^6. In terms of outputs, the uniform flow conditions far downstream of the cascade were obtained, just like in the experiments, via the set of conservation equations explained in Ref. [14] under Sec. 2.4.5.2. However, before presenting the results, it must be noted that many of the simulations performed in these transonic conditions did not fully converge due to perceived periodical numerical instabilities. This may be expected due to the unsteady nature of these operating conditions, especially near choke and stall conditions. When this was the case, care was taken to arithmetically average the results obtained at the following points of interest: inlet, outlet, and blade surface. This averaging was performed over two cycles of the periodic numerical instability, as observed in the mass flow measured at the outlet of the domain.

For the convergence study itself, the process described by Celik et al. in Ref. [39] was carefully followed. To start, three meshes of roughly 35, 65, and 134 thousand faces in the blade-to-blade view were created. These refinement levels compare reasonably as coarse, mid, and fine meshes to the mesh used in the previous URANS study of the TFAST cascade with 54 thousand faces. Simulations were then performed with all three meshes with the numerical setup described. Finally, the absolute total pressure at the outlet was chosen as the critical variable, and the discretization error was estimated following the recommended procedure. The results obtained are summarized in Table 1. From these results, the mid-refinement level was chosen for the purpose of optimization. This level provides the best balance between accuracy, with a Grid Convergence Index (GCI) of 1.01%, and calculation time for the scope of the optimization.

A general overview of the mid-refinement level mesh chosen can be observed in Fig. 4. Most of the refinement can be observed to be focused on the passage area, where the shock is expected, but also in the wake, and in the O- and C-blocks surrounding the airfoil. It can also be noted that for the purpose of the study, the y^+ parameter around the airfoil was maintained under one for all refinement levels. Care was also taken to ensure that the outlet block had a similar orientation as the airfoil's trailing edge. This was observed to help the discretization of the wake far downstream of the airfoil, and therefore the results. Lastly, a total of 34 points were used in the spanwise direction for all meshes in this study. However, a sequential decrease of the number of points down to 7 showed minimal differences in the results obtained. Therefore, the mesh with 65 thousand faces, 7 spanwise points, and a total of 526 thousand elements was used for the rest of the study.

Table 1 Mesh convergence study results

	φ = Absolute total pressure at outlet
N_1, N_2, N_3	134,000, 65,000, 35,000
h_1, h_2, h_3	0.408, 0.518, 0.624 mm
φ_1, φ_2, φ_3	85.15, 85.50, 86.01 kPa
r_{21}, r_3	1.27, 1.20
GCI^{21}, GCI^{32}	0.5%, 1.01%

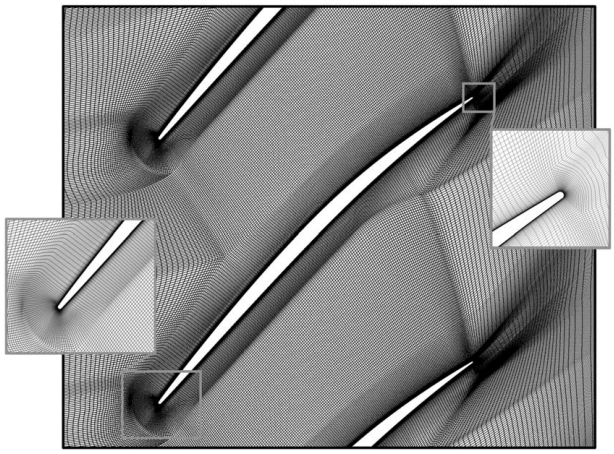

Fig. 4 Reference TFAST cascade mesh with 65 thousand faces

4.3 Comparison Between Computational Fluid Dynamic and Experiment. In this section, the CFD simulations performed with the TFAST cascade are compared directly to the experimental results gathered in Ref. [13]. This step is important to "calibrate" the numerical setup for the optimization, given that the inviscid wall contraction applied at the tip of the blade introduces slight discrepancies in the results with respect to the experiments. Namely, forgoing the discretization of the sidewall boundary layer ignores the energy dissipation that would normally occur because of it, as described in detail in Ref. [40]. Therefore, it was expected that the numerical simulation that best matched the isentropic experiment's Mach number distribution would occur at a slightly different outlet pressure and higher inlet Mach number.

To verify this, a series of simulations were performed at different outlet pressures to compare with the experiment, as shown in Fig. 5. In this figure, it can be observed that applying the same outlet pressure of 57.6 kPa as the experiment provides an overly accelerated isentropic Mach number distribution, with a much higher pre-shock Mach number. On the other hand, an outlet pressure of 62.1 kPa matches the Mach number of 1.2 at the inlet, but it greatly underestimates the isentropic Mach number distribution over the blade surface. Finally, an outlet pressure of 59 kPa was found to provide the best match with the experiment. At this outlet pressure, the main differences observed between the CFD and the experiments are summarized in Table 2. Notably, in the CFD results, the Mach number at the inlet was found to be slightly higher, while the losses and the de Haller number (*DH*) were found to be lower. These comparisons and values obtained were then used to inform the definition of the design point for the optimization, and

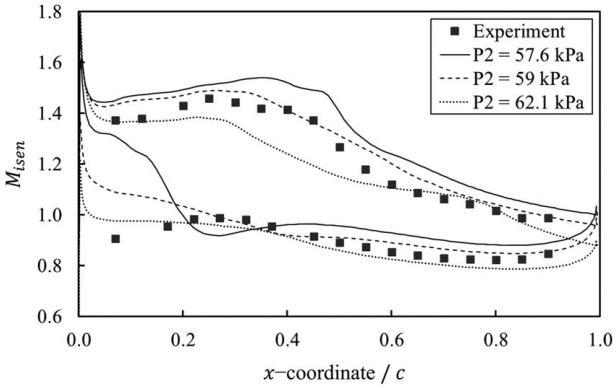

Fig. 5 Isentropic Mach number distribution comparison between TFAST experiment and CFD

Table 2 Results from TFAST experiment and best CFD simulation

	Exp.	CFD
M_1	1.21	1.31
ω	0.149	0.132
DH	0.683	0.628
β_2	130 deg	132.4 deg

the remaining optimization constraints and parameters in the following sections.

5 Cascade Design Strategy

For this optimization, the goal of designing a "state-of-the-art" compressor cascade was defined as a cascade with similar operating conditions, working range, aerodynamic loading, and flow turning as the TFAST cascade from the mesh convergence study. Accordingly, a design strategy was prepared that would capture these performance metrics in order to obtain an appropriate set of cascade candidates from which to choose a final design. In this section, the design strategy is presented starting with the optimization's objective functions, followed by the search for the design point of each cascade candidate, and the procedure to calculate the working range at the design Mach number.

5.1 Objective Functions. In AutoOpti, the objective functions are set to be minimized by the optimizer. Additionally, if there is more than one objective, the optimizer will continuously search the design space for members that improve the Pareto front available. For these reasons, it was decided that a total of two objective functions would be employed focused on different aspects of the cascade performance: the efficiency of the cascade at the DP, and over the WR at the design Mach number. These objectives were then defined as follows:

$$f_1 = \omega DP \tag{1}$$

$$f_2 = \bar{\omega} - \frac{WR}{50} \tag{2}$$

The first objective is then focused directly on minimizing the total pressure loss coefficient at the design point specified. On the other hand, the second objective focuses on minimizing the average total pressure loss coefficient over the working range of the cascade, which is subtracted by a fraction of the working range span itself. This is done in order to reward the cascades with longer working ranges, which is a desired feature in a compressor cascade design. A robust numerical definition and methodology are then required to find the design point and the working range of the cascades for the computation of the objective functions. These strategies are explained in detail in the following sections.

5.2 Design Point Search. The archetypal total pressure loss coefficient polar of a transonic cascade is shown in Fig. 6. In order to start calculating the polar for a given cascade candidate, the design point must be defined based on a number of inlet flow inputs and performance constraints. The inlet flow angle and the absolute total pressure were chosen to be the same as TFAST with 145.5 deg and 93.6 kPa, respectively. The operating point of the cascade was then searched by iterating on the outlet pressure between 57.8 and 60.2 kPa until a de Haller number between 0.62 and 0.65 was obtained. These values indicate a similar aerodynamic loading to the TFAST cascade based on the experience from the previous mesh convergence study. If the de Haller number could not be matched after a maximum of 8 simulations, the member would be considered unconverged, and the process chain would

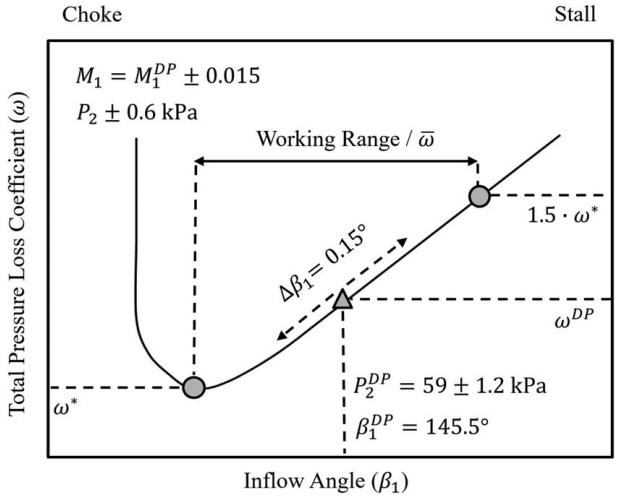

Fig. 6 Total pressure loss coefficient polar definition for the optimization

be finished. If the de Haller number was matched, the results obtained were saved as the design point of the cascade. This point is also constrained to have an inlet Mach number between 1.28 and 1.35, and a *FT* between 11 and 13.5 deg. If any of these constraints are not met, AutoOpti again discards the member as unconverged and the process chain is finished. It is worth noting that all the converged and unconverged members inform the Kriging metamodel, improving the knowledge of the design space with respect to the constraint limits.

It can also be highlighted here that the de Haller number has been chosen as the main metric of aerodynamic loading, instead of the sometimes more commonly used Diffusion Factor (DF). The reason for this decision is the distinct origin of the DF as a metric derived from the correlations obtained with classical NACA airfoils. Indeed, the maximum velocity on the suction surface of these airfoils was correlated with the pitch-to-chord ratio and the easier-to-measure inlet and outlet velocities. This provides a metric that is easy to understand and correlate for designers, but is not as useful for the optimizer, as the Kriging process is able to correlate all the flow and design parameters together. Therefore, it was estimated that a more general aerodynamic loading metric such as the de Haller number would be better than the diffusion factor for this optimization effort that seeks to explore a wide variety of airfoil designs.

5.3 Working Range Search. If the search for the design point of the member is successful, the rest of the total pressure loss coefficient polar must be computed to obtain its working range performance. This is done by iterating on the cascade's inlet flow angle with steps of 0.15 deg above and below the design point inflow angle of 145.5 deg. Over the course of this main iteration, a second one may be performed on the outlet pressure in order to maintain the inlet Mach number within an interval of 0.015 above or below the inlet Mach number at the design point (M^{DP}). This second iteration is performed with step sizes of 200 Pa and a maximum of 6 simulations. At first, the iteration on the inlet flow angle is performed towards the cascade's choke regime until the point of minimum total pressure loss is obtained. This point corresponds to the start of the cascade's unique incidence condition [41]. Afterward, the iteration is continued from the design point towards the stall regime until the cascade has reached a total pressure loss coefficient 50% higher than the minimum previously captured. The working range and the average total pressure loss coefficient over this range are then calculated and passed to the optimizer for the evaluation of the objective functions. This whole process and all the constraints defined are summarized in Fig. 6 and in Table 3.

Table 3 Summarized optimization constraints

	Min.	Max.
t_{max}/c	0.032	0.05
x_{tmax}/c	0.4	0.635
A/c^2	0.021	0.045
x_{cen}/c	0.448	0.544
DH^{DP}	0.62	0.65
M_1^{DP}	1.28	1.35
FT^{DP}	11 deg	13.5 deg

6 Optimization Results

This optimization was powered by the DLR's computational cluster, *CARA*. A total of 1633 process chains were calculated, resulting in 663 converged and 970 unconverged members. The final results of the optimization were confirmed by reviewing the convergence of the Kriging metamodel and performing a sensitivity analysis on the top-ranked member. In this section, the results obtained will be discussed in detail starting with the sensitivity analysis, a discussion on the database of optimized cascades obtained, and a short description of the post-optimization analyses performed in order to arrive at a final cascade choice.

6.1 Sensitivity Analysis. To confirm the convergence, a single parameter sensitivity analysis was performed on the top-ranked member. For this purpose, the design parameters of said cascade were recovered and manually varied one at a time within an interval of 10% of the total range of the parameter in the optimization. The result from this process showed that the member's objective functions did not improve, or if they did, that the constraints were not satisfied anymore. This can be observed in Fig. 7, where the variation of the trailing edge's design parameters is shown to only increase, or at best maintain, the values of both objective functions. In fact, the variation of the parameters down to −10% of the total range causes the first and second objective functions to increase up to 4.5% and 12% of the original member's values, respectively.

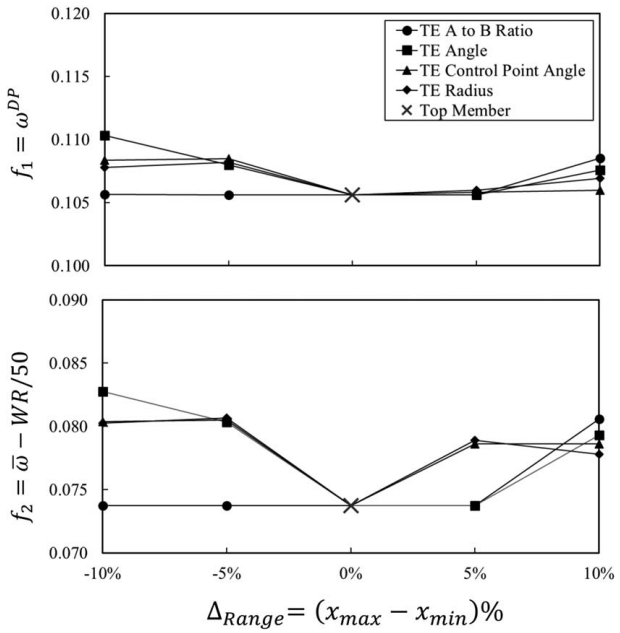

Fig. 7 Sensitivity study performed on the trailing edge design parameters

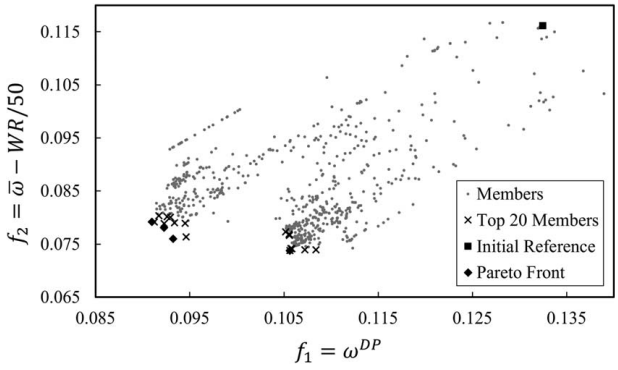

Fig. 8 Resulting database of optimized airfoils

6.2 Resulting Database of Optimized Cascades. The full database of optimized cascades obtained from the optimization is shown in Fig. 8 in terms of objective function performance. It can be observed here that the optimizer has progressively improved the performance of new members with respect to the initial reference shown. This reference corresponds to the TFAST cascade, with only minor modifications to be able to adapt it to the process chain of the optimization. From Fig. 8, it can also be observed that the Pareto front and the top 20 members have converged towards two groups of cascades: the first one on the left optimized to the best possible values of the first objective, and the second one on the right optimized to the best possible values of the second objective.

On the other hand, the optimizer has not been able to find a lot of "middle-ground" designs with satisfactory performance between these two main groups of optimized cascades. In fact, many of the members within this range were observed to fail either one or more of the design point constraints: DH^{DP}, M^{DP}, or FT^{DP}. This however can be understood due to the highly constrained nature of the design space required for optimization of this sort of application. It is thought as well that smaller step sizes within the CFD strategy for the outlet pressure and the inflow angle would have provided a smoother transition between these two main optimized groups. However, this would have considerably increased the computational resources required throughout the optimization, as some members were observed to already require over 50 CFD simulations for a complete process chain. Therefore, the CFD strategy presented was formulated to provide the best balance between these two competing factors.

6.2.1 Geometrical Comparison. In order to start categorizing the types of designs obtained, an initial thickness comparison helps identify two main groups of airfoils: the "thick" airfoils, which achieved the best values for f_1; and the "thin" airfoils, which achieved the best values for f_2. This is based on maximum airfoil thicknesses of about 4.7 and 3.7% of the chord length, respectively. For comparison, the reference airfoil had a maximum thickness of 3.5%. However, an additional distinction can be made within the thick airfoils based on the radius of the trailing edge to define a mid-thickness group, hereon labeled as "mid" airfoils. More precisely, the mid and thick airfoils showed radii of 0.28% and 0.45% of the chord length, respectively. For comparison, the reference airfoil and the thin airfoils have a radius of about 0.19%. Small differences were also observed on some leading-edge parameters such as the angle, and the elliptical parameter. However, many of the other geometrical parameters were converged to one main value. This notably includes a stagger angle of around 135.8 deg, a cascade pitch of 67 mm, and a leading-edge radius of about 3.4% of the chord length.

To further compare and understand the different candidates available, the best members from each of these three main groups are compared in Fig. 9 in terms of their unstaggered geometry and

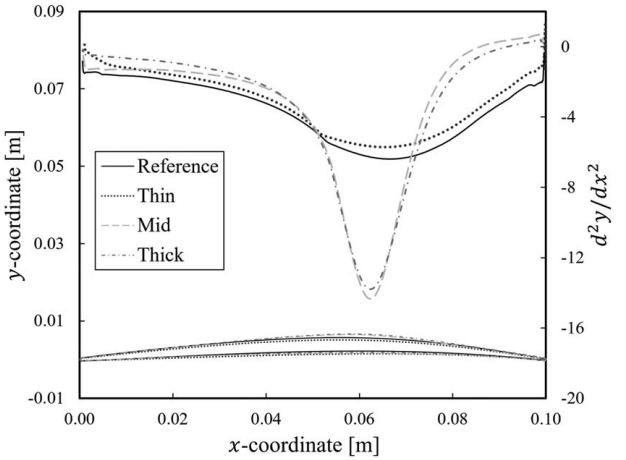

Fig. 9 Geometrical comparison of the best members from the optimization

suction surface curvature. There, it can be observed that the thin airfoil has a curvature distribution very similar to the reference airfoil, with slightly reduced magnitudes. It could be said then that it has been adapted to the somewhat lower aerodynamic loading and flow turning that was allowed in the optimization. On the other hand, the mid and thick airfoils have a very high amount of curvature concentrated at the 60% chord length. Notably, before this point, the curvature of the airfoil is maintained at a very low level. This type of design strategy has been seen in the past, where the low curvature on the front part of the blade allows for a lower pre-shock Mach number and less severe shock.

6.2.2 Design Point Performance Comparison. Due to the fact that this new cascade will not be implemented within the context of a compressor machine, a rigid choke and stall margin constraint was not enforced. Therefore, the working ranges of the cascades are slightly misaligned with respect to the reference. However, a small adjustment to the stagger angle of +0.4 deg, −0.35 deg, and −0.4 deg for the thin, mid, and thick airfoils respectively, allows the direct comparison of all the cascades in terms of performance. The first comparison is performed at the design point with an inlet flow angle of 145.5 deg. At this operating point, the total pressure loss coefficient of the cascades is 0.132, 0.096, 0.101, and 0.103 for the reference, thin, mid, and thick airfoils respectively. Starting with the isentropic Mach number distribution shown in Fig. 10, it can be observed that the optimized airfoils have in general a reduced pre-shock Mach number compared to the reference. The location of the shock is also further downstream of the airfoil. Comparing the different design candidates with each

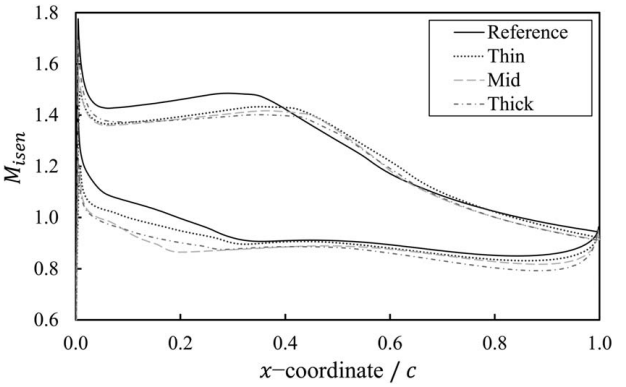

Fig. 10 Isentropic Mach number distribution at design point conditions

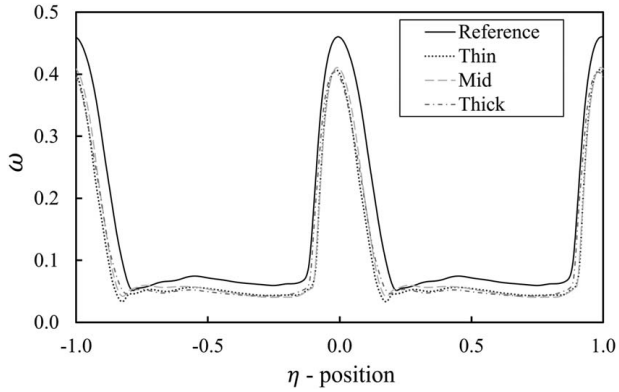

Fig. 11 Outlet total pressure loss coefficient at design point conditions

other, it can be observed that the lower curvature of the mid and thick airfoils helps maintain the pre-shock Mach numbers even lower than the thin airfoil.

For further analysis, the total pressure loss coefficient distribution along the pitch and 30 mm downstream of the cascade are shown in Fig. 11. There, the η-coordinate has been normalized by the pitch and defined to originate at the trailing edge position as projected with the stagger angle. The thin airfoil is shown to have slightly higher losses in the pitch range between 0.50 and 0.75, outside the main wake area. The losses in this area are mainly due to the shock and were expected to be slightly higher from the previous isentropic Mach number distribution analysis. However, the thin airfoil seems slightly better adapted to produce a marginally smaller wake, and from this, a lower overall coefficient than the mid and thick members. In spite of these differences, all cascades show a very similar performance with a loss coefficient of about 0.100. This represents an improvement of about 24% with respect to the reference, which is shown to have a higher peak of total pressure loss and a larger wake area.

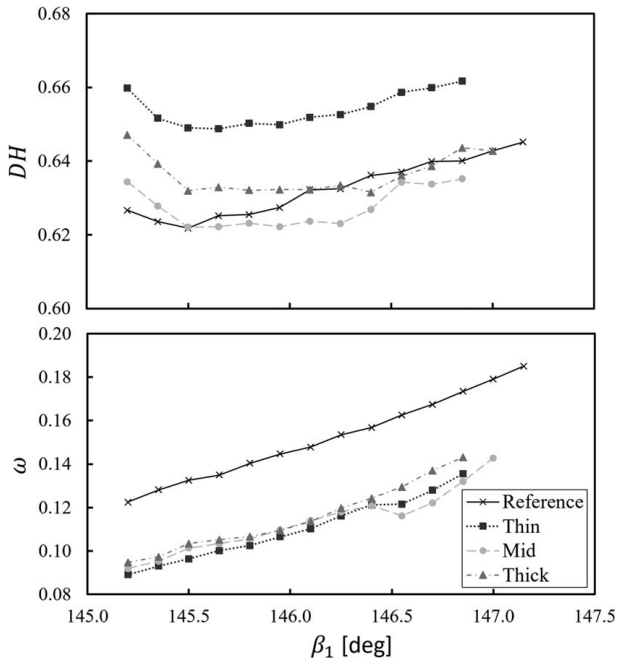

Fig. 12 Total pressure loss coefficient polars and de Haller number performance

6.2.3 Working Range Performance Comparison. The cascades are then compared in terms of their performance over the entire working range in Fig. 12 with the polar for the loss coefficient and de Haller number. In this figure, it can be observed that the new cascades maintain the improvement of total pressure loss throughout the entire range. In fact, near the end of the working range at 146.9 deg, the total pressure loss coefficient for the mid and thin cascades is 0.132 and 0.135, respectively. This represents a 20% improvement compared to the performance of the reference cascade at the same inflow angle. These values are also comparable to the performance of the reference at the design point. The de Haller number comparison also indicates that this improvement has been achieved at relatively similar aerodynamic loading conditions. This is especially the case for the mid cascade, while the thin cascade maintains a difference of about +0.03 units. This comparison helps maintain the improvement of efficiency in context. Similar conclusions can also be drawn with the pressure ratio output of the cascades (not shown). Given that this cascade is not designed to fit into a specific machine, the slight decrease of the aerodynamic loading and flow turning do not represent a significant drawback. However, within a different context of more rigid performance and design margins, this might not always be the case.

6.3 Post-Optimization Analyses. In this section, a brief overview of the different post-optimization analyses performed in order to designate the "best" cascade from the optimization is presented. This is done firstly through a review of the performance of the cascades at off-design operating conditions, and secondly with a final discussion on all the results obtained.

6.3.1 Off-Design Point Performance Study. Within the context of blade design, off-design performance must always be taken into account in order to ensure a robust design that can be used in a compressor machine. These properties would ideally be captured within the process chain and objectives of the optimization itself. However, the CFD process chain would have demanded too many computational resources for the scope of the current optimization's goals. Instead, an off-design performance study was performed on the top cascade candidates to ensure the following general requirements are still met: the cascades have a generally better total pressure loss performance over the working range at comparable aerodynamic loading conditions, and the working range itself is comparable to the reference. These requirements are then in essence the same as the ones enforced in the second objective function of the original optimization. More specific constraints on mass flow or other machine-related properties are not within the scope of the study. Additionally, for this study, the cascades were compared with each other at their original stagger angles. This is given that the comparison is focused on the properties over the whole working range and not at a specific operating point as before.

With the previously defined requirements in mind, Fig. 13 again shows the total pressure loss coefficient and de Haller number polars of all the cascades at an inlet Mach number of 0.85. It can be observed that the optimized cascades were also able to show significantly improved total pressure loss performance throughout the working range at this Mach number. This is especially the case for the mid-airfoil, which shows a minimum total pressure loss coefficient about 24% lower than the minimum of the reference cascade. The working ranges can also be said to be comparable in size. However, at these operating conditions, a greater difference can be observed between the candidate airfoils. For instance, the thick airfoil shows a consistently higher total pressure loss than the mid-airfoil, with a minimum value of only about 8.5% lower than the reference. Finally, the thin airfoil has a minimum total pressure loss comparable to the mid-airfoil, but its performance clearly degrades at higher inflow angles. At these conditions, the performance of the cascade is comparable to the thick airfoil. Therefore, it can be said that the thin airfoil has a shorter working range at this

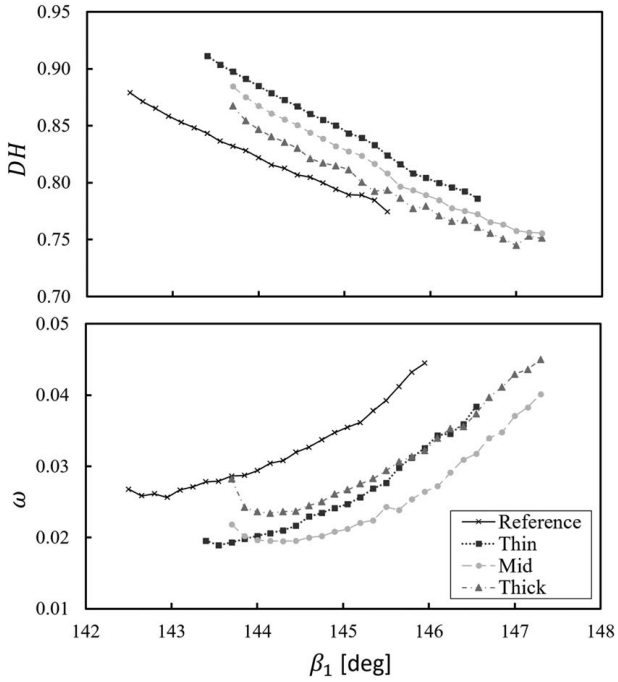

Fig. 13 Cascade performance at 0.85 off-design inlet Mach number

inlet Mach number. Further studies were performed with all cascades at inlet Mach numbers of 1.05 and 1.2. These studies are not shown but showed similar trends with a general improvement of the total pressure loss performance for all cascades with respect to the reference. This improvement however was also generally more clear and consistent for the mid-airfoil than the other candidates.

6.3.2 Best Cascade and Detailed Performance. With all the results gathered and the data analyzed, it is generally clear that the cascade with the mid-thickness airfoil is the most balanced one in terms of performance and working range consistency. This was observed not only at the design Mach number operating conditions but also over the course of the studies at different off-design inlet Mach numbers. Compared to the thick airfoil, the performance of the mid-airfoil was clearly better in most metrics. On the other hand, the thin airfoil also provided good performance at design

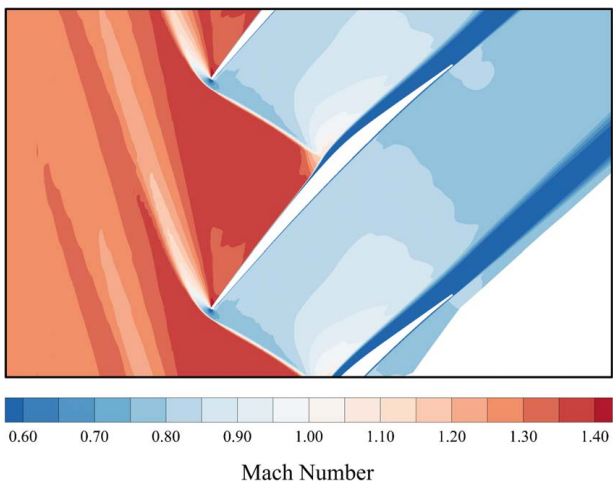

Fig. 14 Mach number contour of cascade member 1532 at design point conditions

Table 4 Summary of cascade member 1532

	Value
β_{st}	135.8 deg
Pitch	67 mm
c	100 mm
M_1^{DP}	1.28
*	0.093
WR	1.95 deg
$\bar{\omega}$	0.112

point conditions, but the performance was observed to degrade away from these conditions. This generally resulted in a shorter working range at these off-design operating conditions when compared with the mid-airfoil cascade. Additionally, within the context of linear cascade wind tunnel testing, the thin profile might be more prone to vibrations, which was not taken into account within the scope of the process chain presented. For these reasons, the mid-airfoil cascade has been accepted as the best possible candidate available for further studies at the DLR related to SBLI in linear transonic compressor cascades. This cascade corresponds to member 1532 from the optimization. A detailed Mach number contour of the cascade at the design point is then given in Fig. 14. In this figure, the general shock structure and flow configuration of the cascade can be observed. Additionally, the main properties and performance of the cascade are summarized in Table 4 for reference. Finally, the exact coordinates of the cascades can be made available to the readers upon request by the authors.

7 Conclusion

In summary, an advanced optimization methodology has been successfully applied to design a new state-of-the-art transonic compressor cascade. For this purpose, a host of in-house DLR software was employed to generate, mesh, and evaluate the performance of new cascade candidates for the DLR optimizer, AutoOpti. A deep review of previous wind tunnel tests at the Transonic Cascade Wind Tunnel informed the optimization strategy, design space, and CFD setup. The optimization's two objective functions were focused on the total pressure loss coefficient at the design point, and over the working range calculated. The final results were validated with sensitivity analysis and provided a database of optimized members with three main groups of thin, mid-thickness, and thick airfoils. These cascades showed up to 24% performance improvement in terms of total pressure loss at design point operating conditions, while maintaining a comparable aerodynamic loading with respect to the reference cascade. Member 1532 from the mid-thickness cascades was determined as the "best" design available because it holds this improvement in off-design operating conditions better than the other candidates.

Most importantly, this design effort demonstrated that the combination of advanced optimization techniques, coupled with robust flow solvers, and a well-targeted optimization strategy still has much to offer to the design of 2D compressor blade sections; especially for compressor machines operating in transonic flow conditions. The general focus in the literature is understandably the design of the entire compressor machine, many times focused on benchmarking them against classical test cases such as NASA's Rotor 37. However, this usually limits the scope of the 2D design of the blade sections, from which there is still much to be learned in terms of design due to the presence of aerodynamic phenomena with mechanisms that are not yet adequately understood nor modeled. Indeed, the results presented confirm that a robust optimization effort focused on a compressor cascade with the best numerical tools available today can still yield significant performance gains with a wide variety of cascade designs.

The design strategy applied also ensures that the cascade selected as the baseline for the rest of the DLR activities within the TEAMAero consortium will offer new and relevant insights to the research and industry community alike. More specifically, the holistic approach planned for this project with wind tunnel tests, high-fidelity simulations, and exploration of flow control methods will aid the fundamental understanding of unsteady SBLI and inform future design methods. Therefore, it is clear that a new chapter has been inaugurated at the DLR, ensuring that the institute remains at the forefront of the research and design of transonic compressor cascades.

Acknowledgment

This project has received funding from the European Union's Horizon 2020 research and innovation program under grant agreement No EC grant 860909. Accordingly, this work has been performed under the framework of the consortium Toward Effective Flow Control and Mitigation of Shock Effects in Aeronautical Applications (TEAMAero). The authors would like to thank Dr. Paweł Flaszynski and the rest of the administration of the TEAMAero consortium for their support that has made the start of this project possible, despite the abnormal circumstances.

Conflict of Interest

There are no conflicts of interest.

Data Availability Statement

The data sets generated and supporting the findings of this article are obtainable from the corresponding author upon reasonable request.

Nomenclature

c = profile chord length
d = perpendicular distance from suction side spline
f = objective function
h = representative mesh size
m = distance along suction side spline
r = edge radius, or grid refinement factor = h_{coarse}/h_{fine}
t = cascade thickness
x = unstaggered airfoil horizontal coordinate
y = unstaggered airfoil vertical coordinate
A = airfoil area
M = Mach number
N = total number of mesh elements
P = pressure
V = flow velocity
AB = A to B elliptical parameter
$AVDR$ = axial velocity density ratio = $\rho_2 V_2 \sin\beta_2/\rho_1 V_1 \sin\beta_1$
DH = De Haller number
FT = flow turning = $\beta_1 - \beta_2$
GCI = grid convergence index
WR = working range in degrees

Greek Symbols

β = Relative flow or geometry angle
η = Normalized pitch coordinate at outlet plane
ω = Total pressure loss coefficient = $(P_{01} - P_{02})/(P_{01} - P_1)$
$\bar{\omega}$ = Averaged total pressure loss coefficient

Sub-and Superscripts

cen = area centroid
DP = design point
$isen$ = isentropic
LE = leading edge
PS = pressure side
SS = suction side
TE = trailing edge
0 = reference state
1 = cascade inlet plane
2 = cascade exit plane
$*$ = value at point of minimum total pressure loss

Abbreviations

CFD = computational fluid dynamics
CP = control point
SBLI = shock-boundary layer interaction
TGK = transonic cascade wind tunnel
TFAST = transition location effect on shock wave boundary layer interaction
URANS = unsteady Reynolds averaged Navier–Stokes

References

[1] John, A., Shahpar, S., and Qin, N., 2016, "Alleviation of Shock-Wave Effects on a Highly Loaded Axial Compressor Through Novel Blade Shaping," Proceedings of the ASME Turbo Expo, Vol. 2A, Seoul, South Korea, June 13–17.
[2] Shahpar, S., 2005, "SOPHY: An Integrated CFD Based Automatic Design Optimisation System," ISABE, Vol. 5, Munich, Germany, Sept. 4–9.
[3] Baert, L., Beaucaire, P., Leborgne, M., Sainvitu, C., and Lepot, I., 2017, "Tackling Highly Constrained Design Problems: Efficient Optimisation of a Highly Loaded Transonic Compressor," Proceedings of the ASME Turbo Expo, Vol. 2C, Charlotte, NC, June 26–30.
[4] Sainvitu, C., Iliopoulou, V., and Lepot, I., 2010, "Global Optimization With Expensive Functions—Sample Turbomachinery Design Application," *Recent Advances in Optimization and Its Applications in Engineering*, Springer, New York.
[5] Benini, E., 2004, "Three-Dimensional Multi-Objective Design Optimization of a Transonic Compressor Rotor," J. Propul. Power, **20**(3), pp. 559–565.
[6] Luo, C., Song, L., Li, J., and Feng, Z., 2012, "A Study on Multidisciplinary Optimization of an Axial Compressor Blade Based on Evolutionary Algorithms," ASME J. Turbomach., **134**(5), p. 054501.
[7] Voß, C., Aulich, M., Kaplan, B., and Nicke, E., 2006, "Automated Multiobjective Optimisation in Axial Compressor Blade Design," Proceedings of the ASME Turbo Expo, Vol. 6B, Barcelona, Spain, May 8–11.
[8] Siller, U., Voß, C., and Nicke, E., 2009, "Automated Multidisciplinary Optimization of a Transonic Axial Compressor," Proceedings of the 47th AIAA Aerospace Sciences Meeting Including the New Horizons Forum and Aerospace Exposition, Orlando, FL, Jan. 5–8.
[9] Aulich, M., and Siller, U., 2011, "High-Dimensional Constrained Multiobjective Optimization of a fan Stage," Proceedings of the ASME Turbo Expo, Vancouver, British Columbia, Canada, June 6–10.
[10] Elfert, M., Weber, A., Wittrock, D., Peters, A., Voss, C., and Nicke, E., 2017, "Experimental and Numerical Verification of an Optimization of a Fast Rotating High-Performance Radial Compressor Impeller," ASME J. Turbomach., **139**(10), p. 101007.
[11] Schnoes, M., and Nicke, E., 2017, "Exploring a Database of Optimal Airfoils for Axial Compressor Design," ASME J. Turbomach., **139**(5), p. 051008.
[12] Youngren, H., and Drela, M., 1991, "Viscous/Inviscid Method for Preliminary Design of Transonic Cascades," Proceedings of the 27th Joint Propulsion Conference, Sacramento, CA, June 24–26.
[13] Hergt, A., Klinner, J., Wellner, J., Willert, C., Grund, S., Steinert, W., and Beversdorff, M., 2019, "The Present Challenge of Transonic Compressor Blade Design," ASME J. Turbomach., **141**(9), p. 091004.
[14] Hirsch, C., 1993, "Advanced Methods for Cascade Testing," AGARDOgraph(AGARD AG 328).
[15] Schreiber, H.-A., 1976, Investigation of Two Transonic Compressor Cascades and Comparison With Rotor Data. Technical Report, Deutsches Zentrum für Luft- und Raumfahrt, Cologne.
[16] Dunker, R. J., Strinning, P. E., and Weyer, H. B., 1977, "Experimental Study of the Flow Field Within a Transonic Axial Compressor Rotor by Laser Velocimetry and Comparison With Through-Flow Calculations," American Society of Mechanical Engineers, Paper No. 77-GT-28.
[17] Dunker, R. J., and Hungenberg, H. G., 1980, "Transonic Axial Compressor Using Laser Anemometry and Unsteady Pressure Measurements," AIAA J., **18**(8), pp. 973–979.
[18] Schreiber, H.-A., and Starken, H., 1981, "Evaluation of Blade Element Performance of Compressor Rotor Blade Cascades in Transonic and low Supersonic Flow Range," Proceedings of the 5th International Symposium on Air Breathing Engines, Bangalore, India, Feb. 16–21, pp. 61–67.
[19] Schreiber, H. A., and Starken, H., 1984, "Experimental Cascade Analysis of a Transonic Compressor Rotor Blade Section," ASME J. Eng. Gas Turbines Power, **106**(2), pp. 288–294.
[20] Starken, H., 1989, "Design Criteria for Optimal Blading Design," AGARD Lecture Series(AGARD-LS-167).

[21] Steinert, W., Fuchs, R., and Starken, H., 1992, "Inlet Flow Angle Determination of Transonic Compressor Cascades," ASME J. Turbomach., **114**(3), pp. 487–493.
[22] Weber, A., Steinert, W., and Starken, H., 1991, "Design and Analysis of a High Pitch to Chord Ratio Cascade Representative of Ducted Propfans," Proceedings of the ASME Turbo Expo, Vol. 1, Orlando, FL, June 3–6.
[23] Nicke, E., Steinert, W., Weber, A., and Starken, H., 1994, "Design and Analysis of a Highly Loaded Transonic Compressor Cascade," AGARD, Montreal, Quebec, Canada, Oct. 4–8.
[24] Weber, A., Schreiber, H. A., Fuchs, R., and Steinert, W., 2001, "3D Transonic Flow in a Compressor Cascade with Shock- Induced Corner Stall," Proceedings of the ASME Turbo Expo, New Orleans, LA, June 4–7.
[25] Weber, A., and Steinert, W., 1997, "Design, Optimization, and Analysis of a High-Turning Transonic Tandem Compressor Cascade," Proceedings of the ASME Turbo Expo, Vol. 1, Orlando, FL, June 2–5.
[26] Weber, A., and Nicke, E., 1997, "A Study of Blade Sweep on the Performance of a Transonic Compressor Cascade with and Without Endwall Influence," Proceedings of the 13th Int. Symposium on Air Breathing Engines (ISABE), Chattanooga, TN, Sept. 8–12.
[27] Hergt, A., Klinner, J., Steinert, W., Grund, S., Beversdorff, M., Giebmanns, A., and Schnell, R., 2015, "The Effect of an Eroded Leading Edge on the Aerodynamic Performance of a Transonic Fan Blade Cascade," ASME J. Turbomach., **137**(2), p. 021006.
[28] Klinner, J., Hergt, A., Grund, S., and Willert, C. E., 2021, "High-Speed PIV of Shock Boundary Layer Interactions in the Transonic Buffet Flow of a Compressor Cascade," Exp. Fluids, **62**(3).
[29] Weber, A., and Sauer, M., 2015, *Pymesh—Meshing Package for Turbomachinery CFD Structured Multiblock Grids: User's Manual*, DLR, Institute of Propulsion Technology, Numerical Methods Group, Cologne.
[30] Starken, H., Schimming, P., and Breugelmans, F. A., 1975, "Investigation of the Axial Velocity Density Ratio in a High Turning Cascade," Proceedings of the ASME Turbo Expo, Houston, TX, Mar. 2–6.
[31] Stark, U., and Hoheisel, H., 1981, "The Combined Effect of Axial Velocity Density Ratio and Aspect Ratio on Compressor Cascade Performance," ASME J. Eng. Power, **103**(1), pp. 247–255.
[32] Schreiber, H. A., and Starken, H., 1982, "On the Definition of the Axial Velocity Density Ratio in Theoretical and Experimental Cascade Investigations," *Measuring Techniques in Transonic and Supersonic Flows in Cascades and Turbomachines*, pp. 1–7.
[33] Becker, K., Heitkamp, K., and Kuegeler, E., 2010, "Recent Progress in A Hybrid-Grid CFD Solver For Turbomachinery Flows," Proceedings Fifth European Conference on Computational Fluid Dynamics ECCOMAS CFD.
[34] Ashcroft, G., Heitkamp, K., and Kuegeler, E., 2010, "High-Order Accurate Implicit Runge-Kutta Schemes for the Simulation of Unsteady Flow Phenomena in Turbomachinery," Proceedings Fifth European Conference on Computational Fluid Dynamics ECCOMAS CFD 2010.
[35] Roe, P. L., 1981, "Approximate Riemann Solvers, Parameter Vectors, and Difference Schemes," J. Comput. Phys., **43**(2), pp. 357–372.
[36] Menter, F. R., Kuntz, M., and Langtry, R., 2003, "Ten Years of Industrial Experience With the SST Turbulence Model," 4th International Symposium on Turbulence Heat and Mass Transfer, Antalya, Turkey, Oct. 12–17.
[37] Langtry, R. B., and Menter, F. R., 2009, "Correlation-Based Transition Modeling for Unstructured Parallelized Computational Fluid Dynamics Codes," AIAA J., **47**(12), pp. 2894–2906.
[38] Doerffer, P., Flaszynski, P., Dussauge, J.-P., Babinsky, H., Grothe, P., Petersen, A., and Billard, F., 2020, *Transition Location Effect on Shock Wave Boundary Layer Interaction: Experimental and Numerical Findings From the TFAST Project, Vol. 144*, 1st ed., Springer Cham, Cham, Switzerland.
[39] Celik, I. B., Ghia, U., Roache, P. J., Freitas, C. J., Coleman, H., and Raad, P. E., 2008, "Procedure for Estimation and Reporting of Uncertainty due to Discretization in CFD Applications," ASME J. Fluids Eng., **130**(7), p. 078001.
[40] Chen, Z., Zhou, M., Xu, Q., and Huang, X., 2018, "A Novel Quasi-3D Method for Cascade Flow Considering Axial Velocity Density Ratio," Int. J. Turbo Jet Engines, **35**(1), pp. 81–94.
[41] Cumpsty, N. A., 1989, *Compressor Aerodynamics*, Longman Scientific & Technical, Essex, UK.